ChemPubSoc Europe

DOI: 10.1002/chem.201405704

CHEMISTRY
A European Journal
Full Paper

Radiolabeling

# $^{99m}$Tc Radiolabeling and Biological Evaluation of Nanoparticles Functionalized with a Versatile Coating Ligand

Michael Felber,[a] Matthias Bauwens,[b] José M. Mateos,[c] Sebastian Imstepf,[a] Felix M. Mottaghy,[b] and Roger Alberto*[a]

**Abstract:** Radiolabeling allows noninvasive imaging by single photon emission computed tomography (SPECT) or positron emission tomography (PET) for assessing the biodistribution of nanostructures. Herein, the synthesis of a new coating ligand for gold nanoparticles (AuNPs) and quantum dots (QDs) is reported. This ligand is multifunctional; it combines the metal chelate with conjugating functions to biological vectors. The concept allows the coupling of any targeting function to the chelator; an example for the prostate specific membrane antigen is given. Derivatized NPs can directly be labeled in one step with $[^{99m}Tc(OH_2)_3(CO)_3]^+$. AuNPs in particular are highly stable, a prerequisite for in vivo studies excluding misinterpretation of the biodistribution data. AuNPs with differing sizes (7 and 14 nm core diameter) were administered intravenously into nude NMRI mice bearing LNCaP xenografts. MicroSPECT images show for both probes rapid clearance from the blood pool through the hepatobiliary pathway. The 7 nm AuNPs revealed a significantly higher bone uptake than the 14 nm AuNPs. The high affinity towards bone mineral is further confirmed in vitro with hydroxyapatite.

## Introduction

The importance of nanoparticles (NPs) for the medical field is rapidly growing.[1] NPs such as mesoporous silica, polymeric NPs, magnetic NPs, gold NPs (AuNPs), and quantum dots (QDs) are promising candidates for the design of new imaging, drug delivery, or theranostic agents.[2] The large surface area to volume ratio distinguishes the properties of NPs from those of bulk materials. It enables the addition of a high payload of functional groups and targeting components on a relatively small volume of material.[3] After their synthesis, NPs are usually coated with hydrophobic surfactants. To render them water soluble, the original surfactants are generally substituted with hydrophilic coating ligands.[4] The nature of these ligands is crucial. In combination with the size of NPs, they determine the interactions in a biosystem as mirrored by the blood retention times, rates of clearance, and potential toxicities.[5] However, as soon as NP formulations are administered to organisms, noninvasive analyses of pharmacokinetics and biodistribution are difficult, especially when NPs do not have an intrinsic contrast property.[6] A very powerful and sensitive method to determine the in vivo behavior of NPs relies on radiolabeling and subsequent detection with single photon emission computed tomography (SPECT) or positron emission tomography (PET).[7]

Radiolabeling of NPs follows essentially two strategies; an "extrinsic" one in which potent, NP surface-bound chelators such as 1,4,7,10-tetraazacyclododecane-1,4,7,10-tetraacetic acid (DOTA) or 1,4,7-triazacyclononane-1,4,7-triacetic acid (NOTA), are directly labeled with $^{64}$Cu or $^{68}$Ga.[7a,8] Alternatively, preformed complexes with bifunctional chelators are subsequently coated to the NP surface.[9] In the "intrinsic" approach, the radiolabel is an integral part of the NP and no additional chelators are required, a concept which has recently been reviewed by Cai and co-workers.[10] $^{99m}$Tc is one of the most commonly used radionuclide for clinical SPECT imaging[11] and NPs were labeled with $^{99m}$Tc. Following the extrinsic, complex-labeling approach, Frangioni and co-workers conjugated preformed $^{99m}$Tc-MAS$_3$ (S-acetylmercaptoacetyl-triserine) to QDs to study the effect of the hydrodynamic diameter (HDD) on the clearance pathway.[9a,12] Torres and co-workers attached preformed $^{99m}$Tc-DPA-ale (dipicolylamine-alendronate) on the surface of iron oxide NPs (IONPs) through a bisphosphonate anchor to obtain bimodal SPECT/magnetic resonance (MR) imaging agents.[9f,13] Cancer receptor-specific AuNPs were labeled with $^{99m}$Tc-HYNIC-derivatives (hydrazinonicotinamide) in a ligand exchange reaction.[9c–e] These labeling procedures require preformation of the $^{99m}$Tc complex and, in a second step, conjugation to NPs through covalent bonds or ligand exchange reactions. For NP drug finding and development, it would be more convenient to label the fully constituted NPs with a complex frag-

[a] M. Felber, S. Imstepf, Prof. Dr. R. Alberto
Department of Chemistry, University of Zürich
Winterthurerstrasse 190, 8057 Zürich (Switzerland)
E-mail: ariel@chem.uzh.ch

[b] Dr. M. Bauwens, Prof. Dr. F. M. Mottaghy
Department of Nuclear Medicine, Maastricht University Medical Center
P. Debeyelaan 25, 6229 Maastricht (The Netherlands)

[c] Dr. J. M. Mateos
Center for Microscopy and Image Analysis
University of Zürich, Winterthurerstrasse 190, 8057 Zürich (Switzerland)

Supporting information for this article is available on the WWW under http://dx.doi.org/10.1002/chem.201405704.

ment that does not require adaption to the chelator or the receptor binding ligand.

Following this strategy, we present herein a new coating ligand for CdSe/ZnS core-shell QDs and AuNPs that allows direct labeling with $[^{99m}Tc(OH_2)_3(CO)_3]^+$ in the last step (Scheme 1).

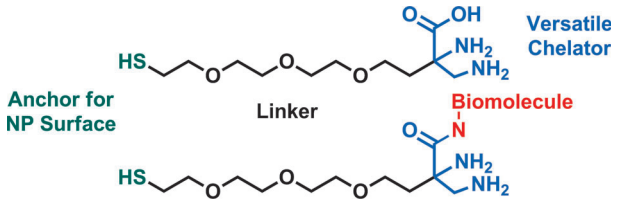


**Scheme 1.** The two multifunctional compounds in the focus of this study.

This ligand comprises functional groups for covalent binding to any biological vector, while underivatized ligands maintain their coordinating properties. A thiol group as an anchor for the NP surface, a polyethylene glycol (PEG) linker and the 2,3-diaminopropionic acid (DAP) chelator for the $[^{99m}Tc(CO)_3]^+$ fragment are part of this ligand. In addition, a small molecule inhibitor for the prostate specific membrane antigen (PSMA) was conjugated to the coating ligand to introduce a targeting function for prostate cancer. After functionalization and radiolabeling of the NPs, the in vitro stability and cellular uptake was examined. Moreover, imaging with small animal microSPECT and ex vivo biodistribution studies in nude NMRI mice harboring LNCaP xenografts were carried out.

## Results and Discussion

### Design and synthesis of the coating ligands

DAP is a small, hydrophilic and very strong chelator for the $[^{99m}Tc(CO)_3]^+$ fragment. It efficiently prevents transmetalation in biological milieu, which may lead to misinterpretation of microSPECT images and biodistribution data. DAP can be derivatized at its α-carbon position, allowing the introduction of functionalities such as linkers to NP surfaces.[14] Conjugation to a PEG linker requires two precursors: Ethyl 2-*N*-(*tert*-butoxycarbonyl)-3-nitriloalaninate **3** and 13-bromo-1-phenyl-2,5,8,11-tetraoxatridecane **5** (Scheme 2).[15] Deprotonation of the tertiary carbon in **3** with NaOEt, subsequent alkylation with **5**, reduction of the nitrile (–CN) with $NaBH_4$ with in situ protection by $(Boc)_2O$ afforded compound **7** (Supporting Information).[14a] Deprotection of the benzyl group and conversion of the resulting hydroxyl group leads to bromide **9**.[15d] The trityl (Trt)-protected thiol was introduced through $S_N2$ displacement of the halide with triphenylmethanethiol to yield **10**. Basic ester hydrolysis of **10** and subsequent deprotection of the Trt- and Boc groups led to the final, multifunctional compound HS-PEG-DAP **12** as a racemate.

Basic ester hydrolysis of **10** gave the carboxylic acid **11**, which can be activated to, for example, compound **18** (Scheme 3). Compound **18** is the central building block in the presented concept. We emphasize the strength of this approach; due to the multiple functions of DAP-based ligand systems, compound **18** can be conjugated to essentially any amine-containing targeting vector. To exemplify this strategy, we selected a small molecule inhibitor of the prostate specific membrane antigen (PSMA), a type II integral membrane protein that is overexpressed on prostate cancer cells.[16] This inhibitor is part of a $^{99m}Tc$ labeled prostate cancer imaging agent and targeted polymeric NPs containing the chemotherapeutic docetaxel, both in clinical trials.[17] Its basic structure is lysine–urea–glutamate.[18] The glutamate moiety is essential for binding to the pharmacophore pocket of PSMA.[19] Therefore, a linker to the ε-amino group of lysine is required. To leave the PSMA binding affinity unaffected, Pomper and co-workers determined 20 Å as the minimum distance between the lysine moiety and a large fragment such as NPs.[20] Consequently, Boc-protected 6-aminohexanoic acid was coupled to the basic inhibitor structure lysine–urea–glutamate.[21] After removal of the protecting groups, compound **17** was conjugated to the NHS-activated carboxylic acid **18** (Scheme 3).

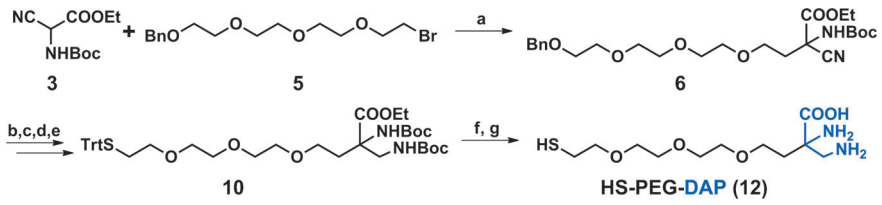


**Scheme 2.** Synthesis of HS-PEG-DAP **12** (only the key steps are shown, the stereochemistry of the DAP-chelating moiety is omitted for simplicity). a) Na, EtOH, heated at reflux, overnight; b) $(Boc)_2O$, $NaBH_4$, $NiCl_2{\cdot}6H_2O$, MeOH, RT, overnight; c) Pd/C (10%), $H_2$ (1 atm), MeOH, RT, overnight; d) $CBr_4$, $PPh_3$, $CH_2Cl_2$, 0 °C–RT, 4 h; e) HSTrt, NaH (60% suspension in oil), THF, heated at reflux, 3 h; f) MeOH/1 M NaOH (1:1), 80 °C, overnight; g) $CH_2Cl_2$/TFA/triethylsilane (TES) (20:8:1.5), RT, 2 h.

We note that linking of the enantiomerically pure inhibitor to racemic **18** leads to a mixture of diastereomers. The two diastereomers could not be separated with preparative high performance liquid chromatography (HPLC). We continued the study without further separation, assuming that the distant (racemic) chelating moiety does not impede the interaction of the enantiomerically pure receptor ligand with the target. The final compound HS-PEG-DAP-TF **20** with the targeting function (TF) was obtained after another deprotection step. In **20**, the distance between the ε-nitrogen of lysine and the thiol-group is 21.3 Å and meets therefore the aforementioned requirements (Supporting Information, Figure S1).

The presented synthetic pathway of compound **12** requires twelve steps when starting from commercially available ethyl cyanoacetate and tetraethylene glycol. Compound **20** can be synthesized in eight steps from the intermediate **11**. The indi-

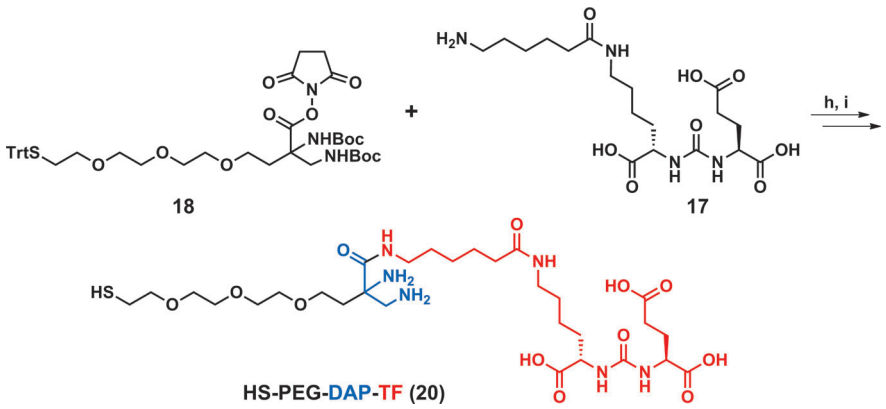


**Scheme 3.** Synthesis of HS-PEG-DAP-TF **20** (only key steps are drawn, the stereochemistry of the DAP-chelating moiety is omitted for simplicity). h) Triethylamine (TEA), DMF/$H_2O$ (4:1), RT, 48 h; i) $CH_2Cl_2$/TFA/TES (20:8:1.5), RT, 2 h.

vidual steps are fast and of good to very good yields (Supporting Information, Experimental Section). Flexibility of the design of this multifunctional ligand system is only restricted for synthetic and analytical reasons by the length of the PEG linker. It is well known that PEGs of molecular weights higher than 2 kDa reduce (undesired) fast clearance through the reticuloendothelial system (RES) by endowing the NPs with "stealth" properties.[22] However, commercially available PEGs of high molecular weights for a reasonable price consist of a distribution of chain lengths, which is not compatible with a well-defined design. Our synthetic procedure, especially careful characterization, requires PEGs with clearly defined chain lengths; hence, we used tetraethylene glycol due to its high purity, which allows silica gel column chromatography separations of single products.

### Synthesis, functionalization, and characterization of NPs

Hydrophobic QDs and AuNPs were synthesized following published procedures.[23] The preparation of oleylamine-stabilized AuNPs limits particle sizes from 6 to 14 nm in diameter. AuNPs with two different core diameters (6.6±0.3 and 13.8±0.4 nm, referred to as $Au^{(7)}$NPs and $Au^{(14)}$NPs in this article, respectively) were synthesized for assessing the size effect throughout biological evaluations (Figure 1 B and C). The characteristic optical property of AuNPs is the surface plasmon resonance (SPR) peak, which was found at 520 nm for $Au^{(7)}$NPs and at 522 nm for $Au^{(14)}$NPs, respectively (Figure 1 E and F).[24] CdSe/ZnS core-shell QDs with a diameter of 6.4±0.1 nm were synthesized to exploit the applicability of the coating ligands **12** and **20** for this NP type (Figure 1 A). Hydrophobic QDs showed the first excitonic peak at 642 nm, an emission maximum at 648 nm and a quantum yield (QY) of 42% (Figure 1 D).

For radiolabeling experiments and biological studies, water solubility of the synthesized NPs is a crucial issue that is achieved by substituting the hydrophobic encapsulation with hydrophilic HS-PEG-DAP (**12**) and HS-PEG-DAP-TF (**20**), respectively. Recently, Mattoussi and co-workers reported a UV-promoted, biphasic approach for the phase transfer of CdSe/ZnS QDs.[25] They applied this method to lipoic acid derivatives and showed a reduction of the disulfide upon UV-excitation, followed by replacement of the hydrophobic capping ligands. Ligands **12** and **20** are not based on lipoic acid but successful phase transfer was still achieved along the same strategy. We note that other commonly applied methods such as biphasic exchange with $CHCl_3$ and phosphate buffered saline (PBS, pH 7.4),[9a] a two-step procedure using histidine as an intermediate coating,[26] or mixing hydrophobic NPs and thiol-ligands in $CH_2Cl_2$ or tetrahydrofuran, all failed. For functionalization, QDs or AuNPs were dispersed in hexane and mixed with an excess of ligands **12** and **20** in methanol for 50 min under UV-irradiation at 365 nm. This photo-mediated ligand exchange led to precipitation of the as-functionalized NPs. The precipitated NPs were isolated, washed with methanol, and re-dispersed in PBS. A 1:1 mixture of **12** and **20** resulted in highly water-soluble NP conjugates. NPs coated with HS-PEG-DAP (**12**) only are poorly soluble in PBS, likely due to the zwitterionic nature of the DAP ligand, which induces electrostatic attractions during the phase transfer and aggregation of NPs. HS-PEG-DAP-TF (**20**) coated NPs expose negatively charged carboxylate groups; electrostatic repulsion provides, thus, good water solubility. To remove any free ligand, the functionalized NPs were finally purified with a PD-10 size-exclusion column.

Phase transfer of QDs did not affect spectroscopic properties such as first excitonic peak or emission maxima (Figure 1 D). The QY dropped from 42 to 10% after phase transfer, attributed to an increased interaction of the QDs with the polar media.[25] A good indication of surface modification and particle aggregation of AuNPs is provided by the SPR peak.[27] The functionalized AuNPs exhibited only a weak bathochromic shift ($\Delta\lambda = 3$ nm) compared with the oleylamine-stabilized AuNPs (Figure 1 E and F). The slight redshifts indicate no significant particle aggregation, which was further supported by dynamic light scattering (DLS) analysis. The NPs are mono-disperse in PBS with an HDD of 13 (QDs), 14 ($Au^{(7)}$NPs), and 20 nm ($Au^{(14)}$NPs), respectively (Supporting Information, Figure S2). The increase of approximately 7 nm for all NPs as compared with the diameter determined in TEM is in agreement with the dimension of the coating ligand HS-PEG-DAP-TF **20** (≈2.8 nm, based on the minimum energy structure; Supporting Information, Figure S1). All three NPs revealed negative ζ-potential values between −21.2 and −22.2 mV in PBS, confirming the negative coating induced by the carboxylate groups of ligand **20**. Functionalization was evidenced by FTIR spectroscopy. The hydrophobic NPs showed typical C–H stretching vibrations of the alkyl chains at 2916 and 2850 $cm^{-1}$ (Supporting Information, Figure S3). Their intensities decreased substantially

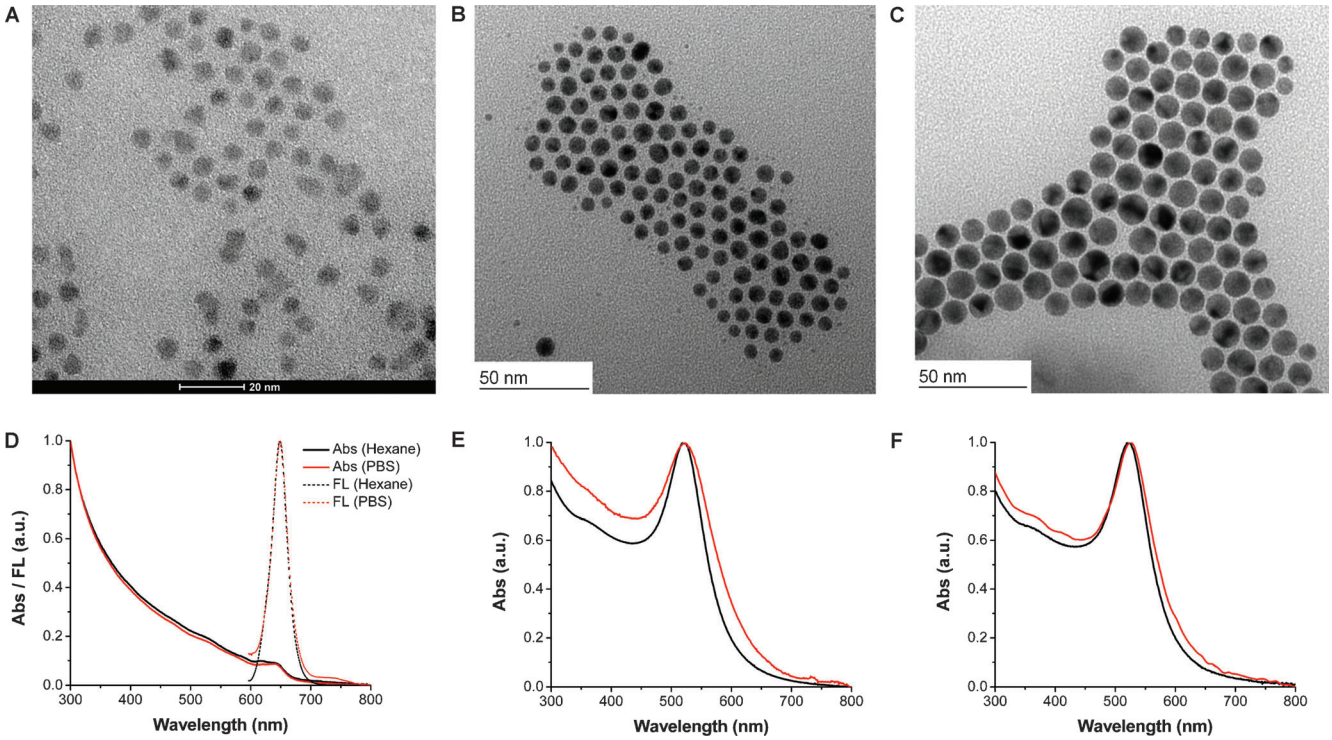


**Figure 1.** Representative TEM micrographs of: A) trioctylphosphine and trioctylphosphine oxide (TOP/TOPO)-coated 6.4 ± 0.1 nm QDs, B) oleylamine-capped 6.6 ± 0.3 nm AuNPs, and C) 13.8 ± 0.4 nm AuNPs (A was recorded with an Eagle CCD camera; B and C were recorded with a Gatan camera). Normalized fluorescence and UV/Vis absorption spectra before (black line, measured in hexane) and after (red line, measured in PBS pH 7.4) functionalization with HS-PEG-DAP (**12**) and HS-PEG-DAP-TF (**20**): D) QDs, E) $Au^{(7)}$NPs, and F) $Au^{(14)}$NPs.

after ligand exchange. The appearance of characteristic urea vibrations in the region between 1626 and 1260 $cm^{-1}$ and a PEG-stretching at 1086 $cm^{-1}$ supported ligand exchange. The relevant analytical data after surface modification are summarized in Table 1.

**Table 1.** Characteristic analytical data of functionalized NPs.

| | QDs | $Au^{(7)}$NPs | $Au^{(14)}$NPs |
|---|---|---|---|
| $\lambda_{max}$ [nm] | 642 (648)[a] | 520 | 522 |
| diameter [nm] | 6.4 ± 0.1 | 6.6 ± 0.3 | 13.8 ± 0.4 |
| HDD [nm] (PDI)[b] | 13 (0.4) | 14 (0.3) | 20 (0.2) |
| ζ-pot. [mV] (STD)[c] | −22.1 (1.9) | −22.2 (2.0) | −21.2 (1.9) |
| $t_R$ [min][d] | 7.01 | 6.21 | 6.14 |
| RCY[e] [%] | 10 | 78 | 49 |
| RCP[f] [%] | ≥95 | ≥95 | ≥95 |

[a] $\lambda_{em}$ [nm]. [b] Polydispersity index. [c] Standard deviation. [d] Size-exclusion HPLC analysis. [e] Radiochemical yield. [f] Radiochemical purity.

## Radiolabeling

The building block for radiolabeling is $[^{99m}Tc(OH_2)_3(CO)_3]^+$, prepared directly from $[^{99m}TcO_4]^-$ (IsoLink).[28] The three water ligands of $[^{99m}Tc(OH_2)_3(CO)_3]^+$ are labile and readily exchangeable with chelators such as DAP. For radiolabeling, a PBS solution of $[^{99m}Tc(OH_2)_3(CO)_3]^+$ was added to NPs dissolved in PBS (final NP concentration 1.0 mg $mL^{-1}$, Figure 2A). The labeling progress was monitored by HPLC, equipped with a size-exclusion column and three detectors (UV/Vis, fluorescence, and gamma counter). Efficient and direct labeling of the NPs is now feasible since DAP is a very strong chelator for the $[^{99m}Tc(CO)_3]^+$ fragment. No separate complex preformation of complexes with NP affine functions and subsequent coating to the NPs is required anymore. Best labeling yields for AuNPs were achieved with a temperature gradient from 50 to 70 °C over 1 h and a subsequent incubation for another hour at 70 °C. Labeling temperature for QDs should not exceed 60 °C since formation of precipitates was observed at higher temperatures.

Chelator and $^{99m}Tc$ complex concentrations are highly dilute. For kinetic reasons, quantitative labeling can thus hardly be achieved in these bimolecular reactions. Estimating the maximum theoretical number of HS-PEG-DAP **12** units on AuNPs results in a ligand concentration between $10^{-5}$ to $10^{-6}$ M for 1 mg $mL^{-1}$ NPs (Supporting Information). This highest concentration is lowered by the actual bound ligand density on the NP surface and by further dilution with the DAP-derived targeting molecule **20**. Therefore, concentrations between $10^{-6}$ and $10^{-7}$ M are a more realistic estimation. $[^{99m}Tc(OH_2)_3(CO)_3]^+$ concentration is between $10^{-8}$ and $10^{-9}$ M, bimolecular reactions become therefore very slow especially with inert $d^6$ centers like the present $Tc^I$ core. Taking these factors into account, the obtained radiochemical yields (RCY) after purification are remarkable and mirror the potency of the DAP chelator (Figure 2B–D, Table 1). If higher temperatures are compatible with NPs, the RCY yields could become quantitative. At the same

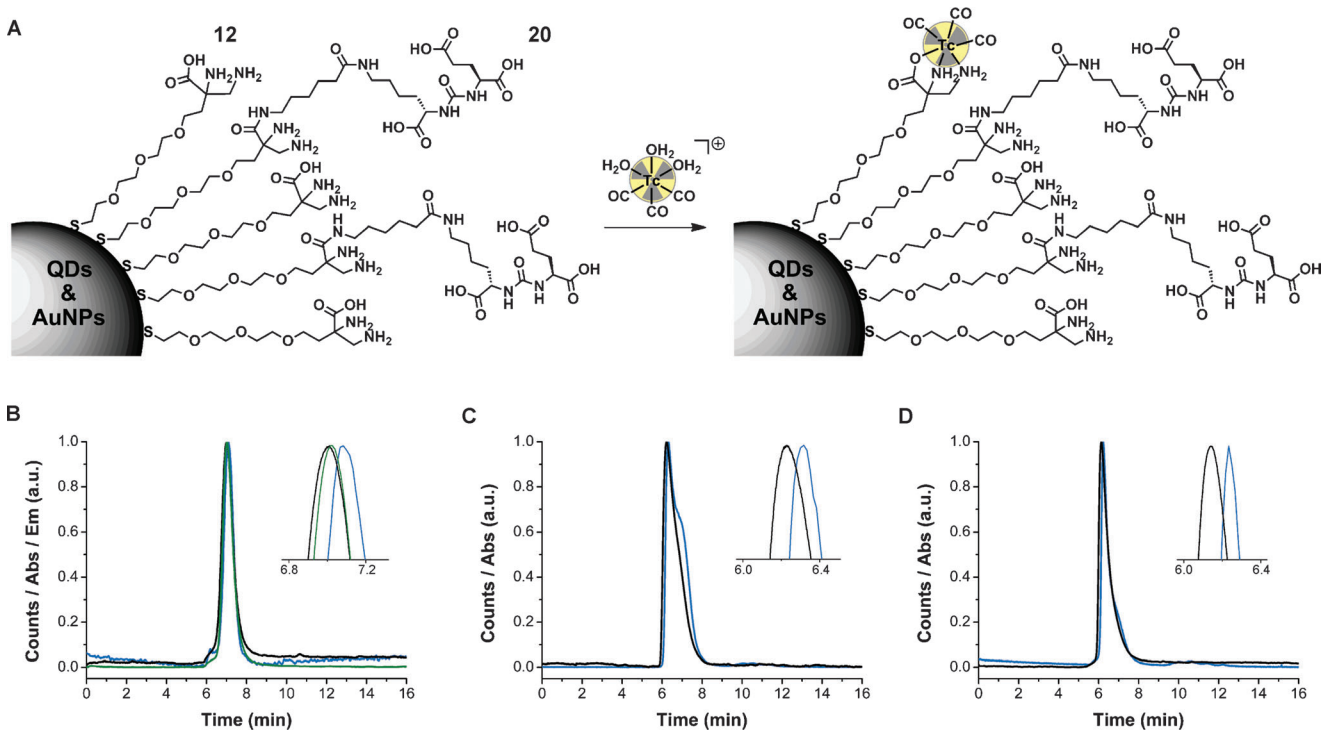


**Figure 2.** A) Radiolabeling scheme of NPs. Normalized HPLC traces of: B) QDs, C) Au$^{(7)}$NPs, and D) Au$^{(14)}$NPs after purification. The analysis includes absorbance at 365 nm (black line), fluorescence at 650 nm (green line), and γ-counts (blue line). Please note that the difference of 0.1 min between the absorbance and γ-counts is due to the detector setup in which the γ-detector is located after the UV-detector.

mg mL$^{-1}$ amounts, Au$^{(7)}$NPs exhibit a higher RCY since the larger surface area as compared to Au$^{(14)}$NPs leads to a higher chelator concentration (for equal amounts of NP) for labeling.

### Chemical and serum stability

For stability assessment, the labeled NPs were kept under air at 40 °C for 12 h in PBS and at 40 °C for 3 h in fetal bovine serum (FBS), whereas the radiolabeled NP solution (10 μL) was mixed with FBS (100 μL). HPLC analysis of the AuNP samples revealed for both stability experiments trace amounts of released $[^{99m}Tc(OH_2)_3(CO)_3]^+$ and $[^{99m}TcO_4]^-$. The radiochemical purity (RCP) was still $>95\%$, underlining the robustness of the DAP complex bound to the AuNP conjugates (Supporting Information, Figure S4B and C). We did not detect released **12** coordinated to the $[^{99m}Tc(CO)_3]^+$ moiety. Labeled QDs are more sensitive and precipitates were observed after 12 h at 40 °C. Centrifugation and HPLC analysis of the supernatant revealed $^{99m}$Tc-labeled HS-PEG-DAP, released as an entity from the QD surface (Supporting Information, Figure S4A). Released coating ligand was also observed in the experiments with FBS. Loss of complex and free ligand from the QDs reduced their hydrophilic character. Exposition of the hydrophobic ZnS shell leads then to precipitation of the QDs. AuNPs did not show this behavior, emphasizing their superior stability over QDs. For long-term stability assessment, NPs were kept in PBS at 4 °C for one week after labeling. Over this period, radioactivity decreased to zero and colloidal stabilities of the now "inactive" NP samples could be studied. DLS and HPLC analyses confirmed that radiolabeling did not affect the HDD of the AuNPs. The optical properties of the AuNPs were preserved and no shift or broadening of the SPR peaks was observed. After one week at 4 °C the QY of the QDs decreased from 10 to 7%, corroborating coating ligand detachment and decreased colloidal stability (see above, and the Supporting Information, Figure S5).[4] This stability problem might be overcome by anchoring the ligands with multiple thiol groups to the surface of QDs.[29] High stabilities are crucial for in vitro and in vivo studies since dissociation of the radiolabel leads to false assessments of the location of the NPs. Hence, we focused on Au$^{(7)}$NPs and Au$^{(14)}$NPs for further biological evaluation.

### Colloidal stability and cellular uptake studies

Having assessed chemical and serum stabilities, colloidal stabilities of NPs under physiological conditions are equally important. The SPR band is very sensitive to changes in the AuNP environment, thus, respective shifts are good indicators for adsorbed serum proteins.[30] Au$^{(7)}$NPs and Au$^{(14)}$NPs in PBS were mixed with FBS and incubated at 37 °C. Insignificant changes in the spectra and SPR band of Au$^{(7)}$NPs indicated little to no interaction with serum proteins, whereas Au$^{(14)}$NPs exhibited a redshift of approximately 1 nm over the period of 24 h (Supporting Information, Figure S6). Shifts of 1 nm are not fully conclusive, therefore, HPLC size-exclusion analyses were performed after 24 h incubation for both probes. Retention times remained unchanged for both AuNPs. In agreement with literature, reporting reduced binding of negatively charged serum

proteins to neutral or negatively charged NP surfaces, substantial blood serum protein binding can therefore be ruled out.[31]

For in vitro evaluation of the NP bioconjugates, we selected the LNCaP cancer cell line, which overexpresses PSMA and is therefore well suited for monitoring uptake by TEM. Literature studies report cellular uptake dependence on NP size, shape, and surface coating.[32] Since the membranes expose an anionic, hydrophilic outer surface, the charge of the NP coating is particularly important.[33] Cationic NPs show generally a higher intracellular uptake as anionic or neutral NPs.[34] Uptake preferences change when NPs are actively transported into the cell, for example, the urea-glutamate targeting function may still efficiently dock to the cell surface-bound PSMA. LNCaP cells were thus incubated with $Au^{(7)}$NPs (179 $\mu g\,mL^{-1}$) and $Au^{(14)}$NPs (189 $\mu g\,mL^{-1}$) for 30 s. After washing and fixing the cells, the samples were embedded in Epon resin to cut ultrathin sections for TEM analysis. The images evidence a localization of AuNPs as black spots on the cell surface (Figure 3 A, B, and Supporting Information, Figure S7a). EDX confirmed the identity of the black spots and control experiments without AuNPs did not exhibit similar black spots in the TEM images (Supporting Information, Figure S7b). The cells were then incubated for 90 min to localize AuNPs within the cells. $Au^{(7)}$NPs were found entrapped in endomembrane compartments, either as single particles or as aggregates (Figure 3 C and D). $Au^{(14)}$NPs were mainly present as single particles in the cytosol without being integrated in endosomes (Supporting Information, Figure S7a). To exclude non-specific uptake of AuNPs, we carried out control experiments under the same conditions with Cos7, a cell line not overexpressing PSMA. None of the TEM images evidenced any AuNPs inside the cells (Supporting Information, Figure S7c), suggesting an active uptake of the AuNPs through the PSMA receptor. Further investigation of the exact uptake mechanism was not carried out at this stage because the main focus was on in vivo evaluation.

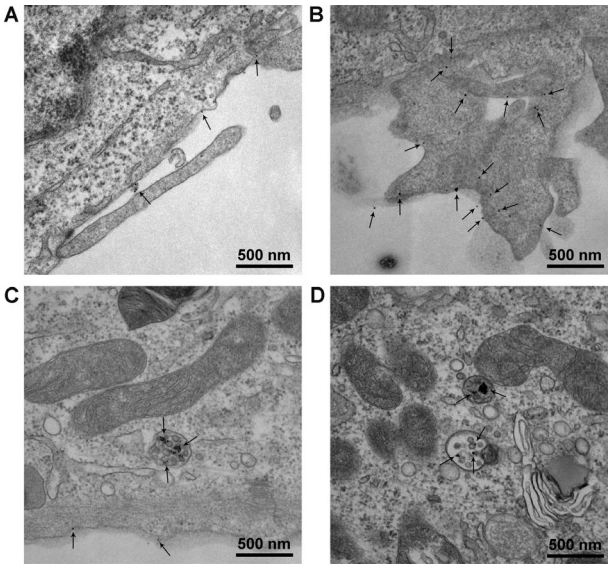


**Figure 3.** Representative TEM images of LNCaP cells after: A, B) 30 s, and C, D) 90 min incubation of $Au^{(7)}$NPs. Due to the high contrast of AuNPs, the sections were used without further contrasting. The location of the AuNPs is indicated with arrows.

### In vivo microSPECT imaging and ex vivo biodistribution studies

The in vivo behavior of the radiolabeled $Au^{(7)}$NPs and $Au^{(14)}$NPs was studied in nude NMRI mice bearing LNCaP tumor xenografts in the region of the left shoulder. After radiolabeling and purification of 1.0 mg AuNPs, the compounds were administered through intravenous injection (i.v.) in concentrations ranging from 50 to 250 μg AuNPs per 0.2 mL injected volume. The ex vivo biodistribution data at 60 min post injection (p.i.) revealed a high uptake in the liver and the spleen for $Au^{(7)}$NPs and $Au^{(14)}$NPs, respectively (Figure 4, detailed % numbers in the Supporting Information, Table S1).

Clearance through the hepatobiliary pathway was expected for both AuNPs based on the HDD and negative surface charge.[35] The radiolabeled NPs showed a low non-specific tissue uptake and tumor uptake was low for both probes. $Au^{(7)}$NPs and $Au^{(14)}$NPs are rapidly cleared to the liver and spleen. Residence time in the circulation is too short for tumor accumulation. MicroSPECT images at an early stage (0–20 min) display almost the entire injected dose in the liver and spleen (Figure 5). The short blood half-life of the compounds indicate quick caption of the NPs by the phagocytic cells of the mononuclear phagocyte system, which consequently decreases the chance of adequate tumor uptake. This could be improved by preparing NP formulations with a neutral surface charge (ζ-potential $\approx \pm 5$ mV),[31c] although this is very challenging with ligand **20** bearing multiple carboxylate functionalities on the very outer surface.

Interestingly, in the early and later (40–60 min) stage microSPECT images of $Au^{(7)}$NPs, the spine, the ribs, and the skull are nicely visualized, features not found for $Au^{(14)}$NPs (Figure 5 and Supporting Information, Figure S8). We first interpreted this observation as uptake by the RES organs, which include the bone marrow. For testing this hypothesis, the femur of the left leg and bone marrow from the spinal column were isolated for ex vivo biodistribution analyses. The bone marrow uptake of $Au^{(7)}$NPs ($0.13 \pm 0.02\,\%ID\,g^{-1}$) and $Au^{(14)}$NPs ($0.12 \pm 0.07\,\%ID\,g^{-1}$) are low and almost identical for both AuNPs. The bone uptake of the $Au^{(7)}$NPs ($3.81 \pm 0.61\,\%ID\,g^{-1}$) on the other hand is significantly higher as compared with the $Au^{(14)}$NPs ($0.88 \pm 0.34\,\%ID\,g^{-1}$). These data are in agreement with the microSPECT images and indicate an interaction with the bone mineral itself rather than an uptake by the bone marrow. More importantly, these are clear indications that overall bone uptake depends on the size of AuNPs, a conclusion that is supported by the biodistribution analyses. Metabolite analysis of the blood plasma and urine should give further insights into the molecular background of this uncommon, size-dependent bone uptake. HPLC analysis of the blood plasma 1 h p.i. showed approximately 50% of radiolabeled $Au^{(7)}$NPs unchanged, but only 7% of the injected $Au^{(14)}$NPs appeared intact (Supporting Information, Figure S9). According to HPLC analyses of the urine, $^{99m}$Tc was mostly present as low molecu-

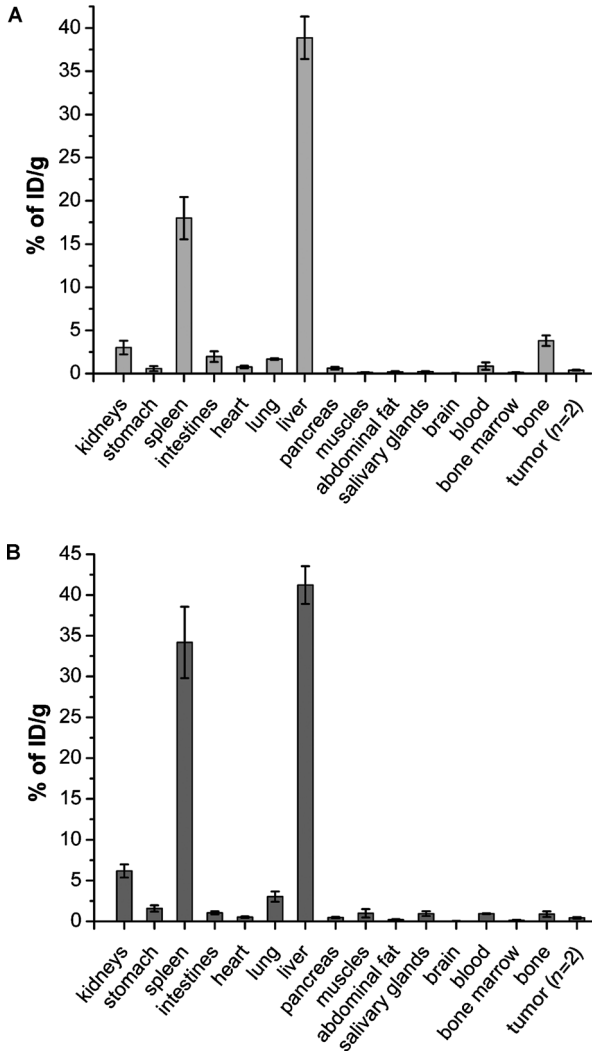


**Figure 4.** Ex vivo biodistribution in LNCaP xenograft mice of: A) $Au^{(7)}$NPs, and B) $Au^{(14)}$NPs, expressed as percentage of injected dose (%ID) per gram organ (mean ± standard deviation, $n = 5$).

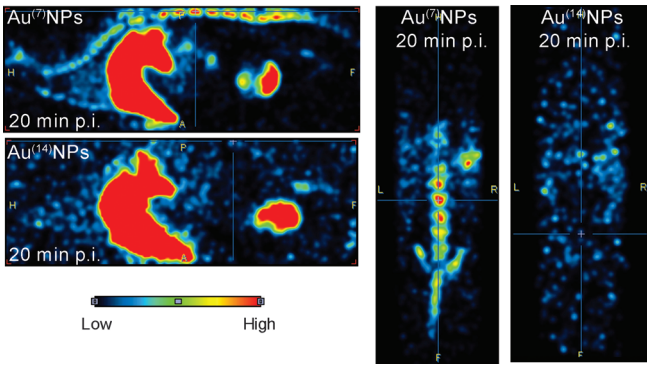


**Figure 5.** In vivo microSPECT images at early scan stage (0–20 min) of $Au^{(7)}$NPs and $Au^{(14)}$NPs (sagittal planes on the left and coronal planes on the right). The injected dose for $Au^{(7)}$NPs probe was 71 MBq and for the $Au^{(14)}$NPs probe 66 MBq.

lar weight species. Metabolites resulting from the NP-coating degradation may be the reason for the uptake in the kidneys since renal clearance of the radiolabeled AuNPs can be ruled out.

According to blood plasma analyses, $Au^{(14)}$NPs are metabolized to a higher degree than $Au^{(7)}$NPs, providing an adequate explanation for the differences in bone accumulation. In vivo degradation of the coating ligands and concomitant loss of the carboxylates has a crucial impact on the surface charge of the AuNPs. Glutamic acid residues in proteins such as osteonectin have a high binding affinity for hydroxyapatite (synthetic analogue for bone mineral).[36] Therefore, the loss of carboxylate groups in the NPs will decrease the affinity for bone minerals. Since Roeder and co-workers suggested glutamic acid-functionalized AuNPs as X-ray contrast agents for damaged bone tissue in a recent study,[37] the affinity of $Au^{(7)}$NPs for bone mineral was assessed with water-insoluble hydroxyapatite. A suspension of hydroxyapatite (2 mg) in a 1.0 mL solution of $Au^{(7)}$NPs (1.0 mg mL$^{-1}$, PBS pH 7.4) was kept at 37 °C and UV/Vis spectra taken at different time points. A constant decrease of the SPR peak and steady decolorization of the solution evidenced binding of the negatively charged AuNPs to the hydroxyapatite surface (Supporting Information, Figure S10).

The microSPECT images together with the quantitative $^{99m}$Tc biodistribution data are a good but not unambiguous indication for intact, radiolabeled $Au^{(7)}$NPs bone binding. These in vivo data could still result from metabolites or radiolabeled ligand leach from $Au^{(7)}$NPs. Only quantitative data on gold distribution, paralleling the one of $^{99m}$Tc, would unambiguously support intact NP binding. Therefore, the Au amount on the femur of the imaged mice shown in Figure 5 was quantified with ICP-MS. The femur of the mice injected with $Au^{(7)}$NPs (71 MBq ID) exhibited an amount of 0.63 μg of Au on the bone (57 mg), whereas 0.11 μg of Au was measured on the femur (51 mg) injected with the $Au^{(14)}$NPs sample (66 MBq ID). These values are fully consistent with the data obtained from the ex vivo biodistribution studies with $^{99m}$Tc and strongly support the affinity of the intact, radiolabeled AuNPs for bone mineral.

## Conclusion

A new coating ligand for thiophilic NPs, containing a terminal thiol group, a PEG linker and the DAP chelator (HS-PEG-DAP) represents a core molecule acting as a chelator and an anchor for targeting functions. The principal affinity for NP surfaces remains thereby unchanged. The biovector conjugation was exemplified with a small molecule PSMA inhibitor, based on the lysine–urea–glutamate sequence (HS-PEG-DAP-TF). AuNPs (7 and 14 nm) and QDs (6 nm) were derivatized with a 1:1 mixture of HS-PEG-DAP/HS-PEG-DAP-TF and directly labeled with $[^{99m}Tc(OH_2)_3(CO)_3]^+$, demonstrating the high potency of the DAP chelator even at high dilution. Whereas derivatized QDs revealed partial detachment of coating ligands, the radiolabeled AuNPs are highly stable. In vitro uptake studies with LNCaP cells and 7 nm and 14 nm AuNPs showed active uptake of AuNPs, indicative for an interaction between the targeting function on the AuNPs and the membrane antigen PSMA. In vivo evaluation in nude NMRI mice harboring LNCaP xeno-

grafts exhibited fast clearance from the blood pool through hepatobiliary excretion and low tumor uptake. Metabolite analysis uncovered a higher stability of 7 nm AuNPs in the blood and a 4–5 times higher bone uptake compared with 14 nm AuNPs. The high affinity for bone mineral was confirmed with in vitro experiments with hydroxyapatite.

In future, the major challenge consists in the design of probes with decent blood retention for tumor accumulation. The conjugation of molecules with tunable surface charges to the HS-PEG-DAP building block will induce prolonged blood retention time of DAP-based coating ligands. Efforts in this direction are currently underway in our laboratories.

## Experimental Section

### Materials, characterization, and synthesis of HS-PEG-DAP (12) and HS-PEG-DAP-TF (20)

A detailed description can be found in the Supporting Information.

### Synthesis of CdSe/ZnS core/shell QDs

CdSe/ZnS core/shell nanocrystals were prepared according to a reported procedure.[23b] Briefly, trioctylphosphine oxide (5 g), hexadecylamine (2.5 g), and trioctylphosphine (1.25 mL) were kept under vacuum at 130 °C for 1 h. Under atmospheric pressure the temperature was elevated to 350 °C. In a separate flask, cadmium acetylacetonate (155 mg), 1,2-hexadecanediol (300 mg), and trioctylphosphine (2.5 mL) were heated under vacuum to 100 °C until the solution became homogeneous. After cooling to 80 °C under atmospheric pressure, 2.5 mL of a 1 M solution of selenium powder in trioctylphosphine (2.5 mL) was added. This mixture with the cadmium and selenium precursors was immediately injected into the 350 °C hot flask and then cooled to 270 °C. At this temperature the mixture was stirred for 60 min and after cooling to room temperature, butanol (50 mL) was added to precipitate the QDs. After centrifugation and removal of the supernatant, the QDs were dispersed in hexane (5 mL) and the precipitation procedure was repeated twice. For the overcoating, trioctylphosphine oxide (30 g) was kept under vacuum at 120 °C for 2 h. The purified CdSe QDs from step 1 were dispersed in hexane (10 mL) and 1 mL of this solution was added to the trioctylphosphine oxide at atmospheric pressure. The solvent was removed under vacuum. At atmospheric pressure, the mixture was heated to 180 °C. In a separate two-neck round-bottom flask trioctylphosphine (4 mL), diethyl zinc (1 M in hexane; 1.0 mL), and hexamethyldisilathiane (180 mg) were mixed and loaded into a syringe. This solution was slowly added to the QD solution and afterwards the temperature was lowered to 80 °C. The mixture was stirred at 80 °C for 2 h and the overcoated QDs were isolated by precipitation with butanol (30 mL) and centrifugation.

### Synthesis of AuNPs

AuNPs were prepared according to a reported procedure.[23a] Briefly, a solution of toluene (49 mL) and oleylamine (2.9 mL) were heated to 115 °C. In a separate flask tetrachloroauric acid trihydrate (60 mg) was dissolved in oleylamine (1.2 mL, 3.7 mmol) and toluene (1 mL). The gold precursor solution was injected in one portion to the boiling solution and the mixture was heated at reflux for 9 (6.6 nm AuNPs) or 130 min (13.8 nm AuNPs). The particle growth was quenched by the addition of methanol (100 mL) and the precipitate was isolated by centrifugation. The product as a black solid was washed three times with methanol and dried in vacuo.

### Functionalization of QDs and AuNPs

The photoinduced phase transfer was adapted from a reported procedure with modifications.[25] Briefly, a mixture of HS-PEG-DAP (7.4 mg, 25 μmol) and HS-PEG-DAP-TF (17.1 mg, 25 μmol) were dissolved in methanol (0.8 mL) and transferred in a nitrogen-flushed glass vial with a magnetic stir bar, sealed with an aluminum crimp cap with a butyl septa. NPs (ca. 1.0 mg) were dispersed in hexane (0.8 mL) and overlaid on the methanol phase. The glass vial was placed in front of a UV lamp (365 nm) and irradiated under vigorous stirring for 50 min. During this procedure, the originally purple hexane phase became completely transparent, whereas the as-functionalized NPs precipitated and the free ligands stayed dispersed in the solvent. The supernatant with excess ligands was removed by decantation. The precipitated NPs were washed with methanol and dispersed in PBS pH 7.4 (0.5 mL). A further purification step was performed with a PD-10 size exclusion and PBS pH 7.4 as a mobile phase. The colored fraction was collected and TEM, UV/Vis, IR, DLS, and ζ-potential analyses were carried out.

### Labeling of functionalized QDs with $[^{99m}Tc(OH_2)_3(CO)_3]^+$

An aqueous solution of $[^{99m}Tc(OH_2)_3(CO)_3]^+$ (0.5 mL, pH 7–8) was added to QDs in PBS pH 7.4 (0.5 mL). The mixture was stirred using a temperature gradient (50–60 °C) over 60 min and additional stirring at 60 °C for 60 min. Radiolabeled QDs were purified with a PD-10 column, whereas only the reddish-colored fraction was collected and analyzed with size-exclusion HPLC.

### Labeling of functionalized AuNPs with $[^{99m}Tc(OH_2)_3(CO)_3]^+$

An aqueous solution of $[^{99m}Tc(OH_2)_3(CO)_3]^+$ (0.5 mL, pH 7–8) was added to purified AuNPs in PBS pH 7.4 (0.5 mL). The mixture was stirred using a temperature gradient (50–70 °C) over 60 min and additional stirring at 70 °C for 60 min. The radiolabeled AuNPs were purified with a PD-10 column, whereas only the purple-colored fraction was collected and analyzed with size-exclusion HPLC.

### Cellular uptake studies

LNCaP (ATCC CRL-1740) and Cos-7 (ATCC CRL-1651) cell lines were purchased from ATCC (France). Both cell lines were cultured according to the ATCC guidelines and seeded on glass coverslips, which were placed in 24-well plates. The cells were incubated with 400 μL AuNP solution (PBS pH 7.4/medium 1:4) for 30 s and 90 min at 37 °C under 5% $CO_2$ atmosphere. The concentration of 7 nm AuNPs was 179 μg mL$^{-1}$ and of 14 nm AuNPs it was 189 μg mL$^{-1}$ (determined by ICP-MS). Control experiments for both incubation times were carried out under the same conditions, but without using AuNP solution. After incubation, the AuNP solutions were removed, the glass coverslips were washed with PBS and transferred into well plates containing 2.5% glutaraldehyde in 0.1 M PB solution. After fixation at 4 °C for 1 h the samples were washed with PBS and incubated in 1% osmium tetroxide in 0.1 M PB at room temperature for 30 min. After washing with water, the cells were dehydrated in an increasing concentration of ethanol (70, 96, and 100%). The cells were infiltrated in a mixture of Epon 812 resin and ethanol (2:1) and finally embedded in pure resin at 60 °C for 60 h. Ultrathin sections (65 nm) were cut with a Reichert Ultracut

and collected on electron microscopy grids. TEM was performed on a Philips CM100.

### In vivo studies and ex vivo biodistribution analysis

All animal experiments were conducted according to the Dutch code of practice for the care and use of animals, after approval from the local animal ethics committee. Animals were male nude NMR mice, both purchased from Harlan (Netherlands) and 12 weeks old at the start of the experiment. For the tumor inoculation LNCaP cells (ATCC CRL-1740) were cultured according to the ATCC guidelines and 1 million cells in 200 μL volume were subcutaneously injected in the left shoulder. Tumors were allowed to grow for 4 weeks, and reached a volume of 0.2–1.0 $cm^3$. The xenograft-bearing mice were anesthetized using isoflurane gas in oxygen (induction 2.5%, maintenance 1.5%) flowing at 2 $L\,min^{-1}$ prior and during the injection of the compounds. The mice were injected through the tail vein with 10–70 MBq radiolabeled AuNPs in 200 μL of PBS pH 7.4. After each study, the mice were sacrificed by intraperitoneal injection of pentobarbital. Blood was collected immediately after sacrifice by cardiac puncture and the other organs/tissues were harvested, weighted, and counted in an automated gamma counter (PerkinElmer Wallac Wizard 1480 automatic gamma). The data are expressed as mean percentage injected dose per gram (%ID $g^{-1}$) ± standard error of the mean.

### MicroSPECT imaging

Single photon emission computed tomography (SPECT) images were obtained on a U-SPECT-II scanner (MILabs) equipped with three γ-detectors. MicroSPECT studies were performed right after i.v. of the radiolabeled AuNPs and the mice were kept anesthetized with 1% isoflurane gas in oxygen flowing at 0.25 $L\,min^{-1}$. The length of the scan was set to 20 min to obtain three sets of data, corresponding to 0–20, 20–40, and 40–60 min p.i. of the tracer. The SPECT data were acquired and reconstructed with the software that is provided with the U-SPECT-II scanner (MILabs). Image analysis was performed with PMOD software (version 2.9, PMOD Inc.).

### Metabolite analysis

Blood samples were withdrawn and immediately transferred into heparinized centrifugation tubes. After centrifugation for 5 min at 2000 g, the separated plasma was directly injected into size-exclusion HPLC. Urine samples were injected directly after isolation without any additional preparation.

## Acknowledgements

We gratefully acknowledge T. Bruggmann, U. Lüthi, G. Barmettler and U. Ziegler from the Center for Microscopy and Image Analysis of the University of Zürich for their support throughout the TEM measurements. We also acknowledge F. Wild from the Department of Chemistry of the University of Zürich for performing ICP-MS measurements. We also thank M. De Saint-Hubert, G. Hendrikx, I. Pooters, S. Voo, and R. Wierts from Maastricht University for their support during the animal studies. M.B. is supported by the Weijerhorst Foundation. The authors declare no competing financial interest.

**Keywords:** gold · nanoparticles · radiochemistry · radiolabeling · technetium

[1] R. Duncan, R. Gaspar, *Mol. Pharm.* **2011**, *8*, 2101 – 2141.
[2] S. Marchesan, M. Prato, *ACS Med. Chem. Lett.* **2013**, *4*, 147 – 149.
[3] a) J. V. Jokerst, S. S. Gambhir, *Acc. Chem. Res.* **2011**, *44*, 1050 – 1060; b) R. Ghosh Chaudhuri, S. Paria, *Chem. Rev.* **2012**, *112*, 2373 – 2433.
[4] N. Erathodiyil, J. Y. Ying, *Acc. Chem. Res.* **2011**, *44*, 925 – 935.
[5] S. T. Kim, K. Saha, C. Kim, V. M. Rotello, *Acc. Chem. Res.* **2013**, *46*, 681 – 691.
[6] C. Pérez-Campaña, V. Gomez-Vallejo, M. Puigivila, A. Martin, T. Calvo-Fernandez, S. E. Moya, R. F. Ziolo, T. Reese, J. Llop, *ACS Nano* **2013**, *7*, 3498 – 3505.
[7] a) F. Chen, H. Hong, Y. Zhang, H. F. Valdovinos, S. X. Shi, G. S. Kwon, C. P. Theuer, T. E. Barnhart, W. B. Cai, *ACS Nano* **2013**, *7*, 9027 – 9039; b) T. Lammers, S. Aime, W. E. Hennink, G. Storm, F. Kiessling, *Acc. Chem. Res.* **2011**, *44*, 1029 – 1038.
[8] a) W. B. Cai, K. Chen, Z. B. Li, S. S. Gambhir, X. Y. Chen, *J. Nucl. Med.* **2007**, *48*, 1862 – 1870; b) M. L. Schipper, Z. Cheng, S. W. Lee, L. A. Bentolila, G. Iyer, J. H. Rao, X. Y. Chen, A. M. Wul, S. Weiss, S. S. Gambhir, *J. Nucl. Med.* **2007**, *48*, 1511 – 1518; c) D. W. Hwang, H. Y. Ko, S. K. Kim, D. Kim, D. S. Lee, S. Kim, *Chem. Eur. J.* **2009**, *15*, 9387 – 9393; d) W. Lu, G. D. Zhang, R. Zhang, L. G. Flores, Q. Huang, J. G. Gelovani, C. Li, *Cancer Res.* **2010**, *70*, 3177 – 3788; e) Y. C. Wang, Y. J. Liu, H. Luehmann, X. H. Xia, P. Brown, C. Jarreau, M. Welch, Y. N. Xia, *ACS Nano* **2012**, *6*, 5880 – 5888; f) S. H. Li, B. Goins, L. J. Zhang, A. D. Bao, *Bioconjugate Chem.* **2012**, *23*, 1322 – 1332; g) J. Frigell, I. Garcia, V. Gomez-Vallejo, J. Llop, S. Penades, *J. Am. Chem. Soc.* **2014**, *136*, 449 – 457.
[9] a) H. Soo Choi, W. Liu, P. Misra, E. Tanaka, J. P. Zimmer, B. I. Ipe, M. G. Bawendi, J. V. Frangioni, *Nat. Biotechnol.* **2007**, *25*, 1165 – 1170; b) R. Torres Martin de Rosales, R. Tavare, R. L. Paul, M. Jauregui-Osoro, A. Protti, A. Glaria, G. Varma, I. Szanda, P. J. Blower, *Angew. Chem. Int. Ed.* **2011**, *50*, 5509 – 5513; *Angew. Chem.* **2011**, *123*, 5623 – 5627; c) E. Morales-Avila, G. Ferro-Flores, B. E. Ocampo-Garcia, L. M. De Leon-Rodriguez, C. L. Santos-Cuevas, R. Garcia-Becerra, L. A. Medina, L. Gomez-Olivan, *Bioconjugate Chem.* **2011**, *22*, 913 – 922; d) B. E. Ocampo-García, F. D. Ramirez, G. Ferro-Flores, L. M. De Leon-Rodriguez, C. L. Santos-Cuevas, E. Morales-Avila, C. A. de Murphy, M. Pedraza-Lopez, L. A. Medina, M. A. Camacho-Lopez, *Nucl. Med. Biol.* **2011**, *38*, 1 – 11; e) B. Ocampo-García, G. Ferro-Flores, E. Morales-Avila, F. D. Ramirez, *Nucl. Med. Commun.* **2011**, *32*, 1095 – 1104; f) L. Sandiford, A. Phinikaridou, A. Protti, L. K. Meszaros, X. J. Cui, Y. Yan, G. Frodsham, P. A. Williamson, N. Gaddum, R. M. Botnar, P. J. Blower, M. A. Green, R. T. M. de Rosales, *ACS Nano* **2013**, *7*, 500 – 512.
[10] S. Goel, F. Chen, E. B. Ehlerding, W. Cai, *Small* **2014**, *10*, 3825 – 3830.
[11] M. R. A. Pillai, A. Dash, F. F. Knapp, *J. Nucl. Med.* **2013**, *54*, 313 – 323.
[12] H. S. Choi, B. I. Ipe, P. Misra, J. H. Lee, M. G. Bawendi, J. V. Frangioni, *Nano Lett.* **2009**, *9*, 2354 – 2359.
[13] R. Torres Martin de Rosales, R. Tavare, A. Glaria, G. Varma, A. Protti, P. J. Blower, *Bioconjugate Chem.* **2011**, *22*, 455 – 465.
[14] a) Y. Liu, B. L. Oliveira, J. D. G. Correia, I. C. Santos, I. Santos, B. Spingler, R. Alberto, *Org. Biomol. Chem.* **2010**, *8*, 2829 – 2839; b) Y. J. Shen, M. Schottelius, K. Zelenka, M. De Simone, K. Pohle, H. Kessler, H. J. Wester, P. Schmutz, R. Alberto, *Bioconjugate Chem.* **2013**, *24*, 26 – 35.
[15] a) G. Yu, S. Z. Wang, K. Wang, Y. F. Hu, H. W. Hu, *Synthesis* **2004**, 1021 – 1028; b) J. W. G. De Meester, H. C. Vanderplas, W. J. Middelhoven, *J. Heterocycl. Chem.* **1987**, *24*, 441 – 451; c) E. P. Balskus, E. N. Jacobsen, *J. Am. Chem. Soc.* **2006**, *128*, 6810 – 6812; d) Z. X. Jiang, Y. B. Yu, *Synthesis* **2008**, 215 – 220.
[16] N. Schulke, O. A. Varlamova, G. P. Donovan, D. S. Ma, J. P. Gardner, D. M. Morrissey, R. R. Arrigale, C. C. Zhan, A. J. Chodera, K. G. Surowitz, P. J. Maddon, W. D. W. Heston, W. C. Olson, *Proc. Natl. Acad. Sci. USA* **2003**, *100*, 12590 – 12595.
[17] a) S. M. Hillier, K. P. Maresca, G. Lu, R. D. Merkin, J. C. Marquis, C. N. Zimmerman, W. C. Eckelman, J. L. Joyal, J. W. Babich, *J. Nucl. Med.* **2013**, *54*, 1369 – 1376; b) J. Hrkach, D. Von Hoff, M. M. Ali, E. Andrianova, J. Auer, T. Campbell, D. De Witt, M. Figa, M. Figueiredo, A. Horhota, S. Low, K. McDonnell, E. Peeke, B. Retnarajan, A. Sabnis, E. Schnipper, J. J. Song, Y. H. Song, J. Summa, D. Tompsett, G. Troiano, T. V. Hoven, J. Wright, P.

LoRusso, P. W. Kantoff, N. H. Bander, C. Sweeney, O. C. Farokhzad, R. Langer, S. Zale, *Sci. Transl. Med.* **2012**, *4*, 1 – 11.

[18] J. W. Babich, C. N. Zimmerman, K. P. Maresca (Molecular Insight Pharmaceuticals), WO2008058192-A2; US2008193381-A1; WO2008058192-A3; TW200836765-A; IN200901787-P2; AU2007316391-A1; EP2097111-A2; CA2669127-A1; JP2010509358-W; CN101778910-A; US2012208988-A1; US2012269726-A1; US8487129-B2; AU2007316391-B2.

[19] C. Barinka, M. Rovenska, P. Mlcochova, K. Hlouchova, A. Plechanovova, P. Majer, T. Tsukamoto, B. S. Slusher, J. Konvalinka, J. Lubkowski, *J. Med. Chem.* **2007**, *50*, 3267 – 3273.

[20] S. R. Banerjee, M. Pullambhatla, Y. Byun, S. Nimmagadda, C. A. Foss, G. Green, J. J. Fox, S. E. Lupold, R. C. Mease, M. G. Pomper, *Angew. Chem. Int. Ed.* **2011**, *50*, 9167 – 9170; *Angew. Chem.* **2011**, *123*, 9333 – 9336.

[21] S. Buchini, A. Buschiazzo, S. G. Withers, *Angew. Chem. Int. Ed.* **2008**, *47*, 2700 – 2703; *Angew. Chem.* **2008**, *120*, 2740 – 2743.

[22] L. H. Reddy, J. L. Arias, J. Nicolas, P. Couvreur, *Chem. Rev.* **2012**, *112*, 5818 – 5878.

[23] a) H. Hiramatsu, F. E. Osterloh, *Chem. Mater.* **2004**, *16*, 2509 – 2511; b) A. R. Clapp, E. R. Goldman, H. Mattoussi, *Nat. Protoc.* **2006**, *1*, 1258 – 1266.

[24] J. M. Slocik, M. O. Stone, R. R. Naik, *Small* **2005**, *1*, 1048 – 1052.

[25] G. Palui, T. Avellini, N. Q. Zhan, F. Pan, D. Gray, I. Alabugin, H. Mattoussi, *J. Am. Chem. Soc.* **2012**, *134*, 16370 – 16378.

[26] J. Zylstra, J. Amey, N. J. Miska, L. S. Pang, C. R. Hine, J. Langer, R. P. Doyle, M. M. Maye, *Langmuir* **2011**, *27*, 4371 – 4379.

[27] J. Tournebize, A. Boudier, A. Sapin-Minet, P. Maincent, P. Leroy, R. Schneider, *ACS Appl. Mater. Interfaces* **2012**, *4*, 5790 – 5799.

[28] R. Alberto, K. Ortner, N. Wheatley, R. Schibli, A. P. Schubiger, *J. Am. Chem. Soc.* **2001**, *123*, 3135 – 3136.

[29] a) E. Gravel, C. Tanguy, E. Cassette, T. Pons, F. Knittel, N. Bernards, A. Garofalakis, F. Duconge, B. Dubertret, E. Doris, *Chem. Sci.* **2013**, *4*, 411 – 417; b) N. Zhan, G. Palui, M. Safi, X. Ji, H. Mattoussi, *J. Am. Chem. Soc.* **2013**, *135*, 13786 – 13795.

[30] a) I. Ojea-Jiménez, L. Garcia-Fernandez, J. Lorenzo, V. F. Puntes, *ACS Nano* **2012**, *6*, 7692 – 7702; b) N. Oh, J.-H. Park, *ACS Nano* **2014**, *8*, 6232 – 6241.

[31] a) F. Alexis, E. Pridgen, L. K. Molnar, O. C. Farokhzad, *Mol. Pharm.* **2008**, *5*, 505 – 515; b) B. Wang, X. He, Z. Y. Zhang, Y. L. Zhao, W. Y. Feng, *Acc. Chem. Res.* **2013**, *46*, 761 – 769; c) J. V. Jokerst, T. Lobovkina, R. N. Zare, S. S. Gambhir, *Nanomedicine* **2011**, *6*, 715 – 728; d) T. Sun, Y. S. Zhang, B. Pang, D. C. Hyun, M. Yang, Y. Xia, *Angew. Chem. Int. Ed.* **2014**, *53*, 12320 – 12364; *Angew. Chem.* **2014**, *126*, 12520 – 12568.

[32] a) E. C. Cho, Q. Zhang, Y. N. Xia, *Nat. Nanotechnol.* **2011**, *6*, 385 – 391.

[33] Y. Qiu, Y. Liu, L. M. Wang, L. G. Xu, R. Bai, Y. L. Ji, X. C. Wu, Y. L. Zhao, Y. F. Li, C. Y. Chen, *Biomaterials* **2010**, *31*, 7606 – 7619.

[34] K. Saha, S. T. Kim, B. Yan, O. R. Miranda, F. S. Alfonso, D. Shlosman, V. M. Rotello, *Small* **2013**, *9*, 300 – 305.

[35] S. Sharifi, S. Behzadi, S. Laurent, M. L. Forrest, P. Stroeve, M. Mahmoudi, *Chem. Soc. Rev.* **2012**, *41*, 2323 – 2343.

[36] M. E. Bolander, M. F. Young, L. W. Fisher, Y. Yamada, J. D. Termine, *Proc. Natl. Acad. Sci. USA* **1988**, *85*, 2919 – 2923.

[37] Z. Y. Zhang, R. D. Ross, R. K. Roeder, *Nanoscale* **2010**, *2*, 582 – 586.

[38] T. W. Baughman, J. C. Sworen, K. B. Wagener, *Tetrahedron* **2004**, *60*, 10943 – 10948.

Received: October 17, 2014
Revised: February 12, 2015
Published online on ■■ ▮▮, 2015

# FULL PAPER

**Radiolabeling in a direct way**: A new bifunctional coating ligand for nanoparticles (NPs) allows fast and efficient radiolabeling with $[^{99m}Tc(OH_2)_3(CO)_3]^+$ (see figure; DAP = 2,3-diaminopropionic acid). A particular focus lies on stability experiments of the radiolabeled probes, both in vitro and in vivo. Metabolite analysis revealed a superior stability of functionalized 7 nm AuNPs as compared with 14 nm AuNPs, which might cause different bone uptake behavior as shown in this study.

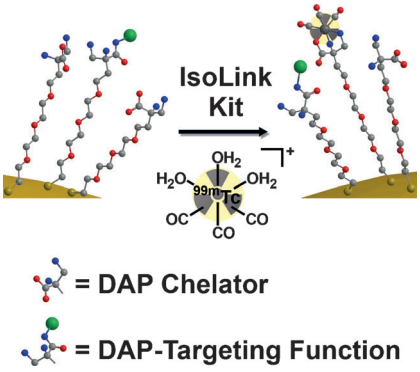


**Radiolabeling**

*M. Felber, M. Bauwens, J. M. Mateos, S. Imstepf, F. M. Mottaghy, R. Alberto**

■■ – ■■

**$^{99m}$Tc Radiolabeling and Biological Evaluation of Nanoparticles Functionalized with a Versatile Coating Ligand**